




Article

Grey Wolf Optimizer with Behavior Considerations and Dimensional Learning in Three-Dimensional Tooth Model Reconstruction

Ritipong Wongkhuenkaew ¹, Sansanee Auephanwiriyaikul ^{2,*}, Marasri Chaiworawitkul ³,
Nipon Theera-Umpom ⁴ and Uklid Yeasarapat ⁵

¹ Department of Computer Engineering, Faculty of Engineering, Biomedical Engineering Institute, Biomedical Engineering and Innovation Research Center, Chiang Mai University, Chiang Mai 50200, Thailand; ritipong.w@cmu.ac.th

² Department of Computer Engineering, Faculty of Engineering, Excellence Center in Infrastructure Technology and Transportation Engineering, Biomedical Engineering Institute, Biomedical Engineering and Innovation Research Center, Chiang Mai University, Chiang Mai 50200, Thailand

³ Orthodontics and Pediatric Dentistry Department, Faculty of Dentistry, Chiang Mai University, Chiang Mai 50200, Thailand; marasri.chai@cmu.ac.th

⁴ Department of Electrical Engineering, Faculty of Engineering, Biomedical Engineering Institute, Biomedical Engineering and Innovation Research Center, Chiang Mai University, Chiang Mai 50200, Thailand; nipon.t@cmu.ac.th

⁵ Department of Computer Engineering, Faculty of Engineering, Chiang Mai University, Empress Dental Care Clinic, Chiang Mai 50200, Thailand; uklid_y@cmu.ac.th

* Correspondence: sansanee@eng.cmu.ac.th; Tel.: +66-5394-2023

Abstract: Three-dimensional registration with the affine transform is one of the most important steps in 3D reconstruction. In this paper, the modified grey wolf optimizer with behavior considerations and dimensional learning (BCDL-GWO) algorithm as a registration method is introduced. To refine the 3D registration result, we incorporate the iterative closest point (ICP). The BCDL-GWO with ICP method is implemented on the scanned commercial orthodontic tooth and regular tooth models. Since this is a registration from multi-views of optical images, the hierarchical structure is implemented. According to the results for both models, the proposed algorithm produces high-quality 3D visualization images with the smallest mean squared error of about 7.2186 and 7.3999 μm^2 , respectively. Our results are compared with the statistical randomization-based particle swarm optimization (SR-PSO). The results show that the BCDL-GWO with ICP is better than those from the SR-PSO. However, the computational complexities of both methods are similar.

Keywords: grey wolf optimizer (GWO); oral healthcare; iterative closest point (ICP); 3D image registration; hierarchical registration; 3D tooth model reconstruction



Citation: Wongkhuenkaew, R.; Auephanwiriyaikul, S.; Chaiworawitkul, M.; Theera-Umpom, N.; Yeasarapat, U. Grey Wolf Optimizer with Behavior Considerations and Dimensional Learning in Three-Dimensional Tooth Model Reconstruction. *Bioengineering* **2024**, *11*, 254. <https://doi.org/10.3390/bioengineering11030254>

Academic Editors: Cosimo Ieracitano and Xuejun Zhang

Received: 26 December 2023

Revised: 25 February 2024

Accepted: 1 March 2024

Published: 5 March 2024



Copyright: © 2024 by the authors. Licensee MDPI, Basel, Switzerland. This article is an open access article distributed under the terms and conditions of the Creative Commons Attribution (CC BY) license (<https://creativecommons.org/licenses/by/4.0/>).

1. Introduction

Three-dimensional reconstruction from multi-view images has been used in many applications, including in orthodontics. It is also used in diagnostic and treatment planning processes in adults and children with dental caries [1,2], especially dental caries that are a cause of chronic diseases in children [3]. With recent technology, e.g., laser or CT, there are several 3D reconstructions from multimodal images research works [4–9] from those technologies. However, in rural areas, there is limited access to these sophisticated devices and also insufficient oral healthcare [10]. In Thailand, the Dental Innovation Foundation, under royal patronage, has provided dental care access in rural communities for a long time. Due to limited access to sophisticated devices in those communities, taking multi-view teeth images inside children's mouths is a very difficult task. Hence, multi-view teeth optical images are collected to be utilized in the 3D reconstruction system. In 3D reconstruction from multi-view images, there are several processes, including image

registration, which is the transforming process of different sets of data into one coordinate system. There are existing works on 2D medical image registration [11–26]. Since point cloud coordinates are used in our 3D teeth reconstruction, the 3D registration is more proper. In the literature, there are several works on 3D registration [27–31] utilizing several features in the registration process, including point cloud coordinates representing the 3D shapes of objects [32–37]. These mentioned works used a variation swarm optimization (PSO) in the location matching between the source and target images. In the hope of improving the registration accuracy, there was study conducted on using the grey wolf optimizer (GWO) instead of PSO in 3D registration [38]. However, only rotation and/or translation were used in those matching locations. Hence, in our previous work [39], the statistical randomization-based particle swarm optimization (SR-PSO) algorithm with the iterative closet point (ICP) method was used to find the optimal affine transform (translation, scaling, rotation, and shearing (shortened from a shearing mapping that displaces each point in a fixed direction by an amount proportional to its signed distance from a given line parallel to that direction)) between teeth optical images.

In particular, a system with the 3D registration using a modified grey wolf optimizer that can reconstruct a 3D image from teeth optical images is developed. However, due to a research ethical approval requirement, we will not use real images taken from children. Hence, we postulate scanned images from two commercial tooth models and then create point cloud images [39]. To avoid premature convergence and to balance between exploration and exploitation, we modify the grey wolf optimization algorithm [40] with behavior considerations and dimensional learning strategies [41–44], called BCDL-GWO, to find the suitable affine transform between the source and target images. This can also enhance global and local searching and improve an ability to escape from a local optima. It has been shown in [41–44] that the BCDL-GWO is a good optimization tool when used to find suitable parameters in several applications, including engineering design problems (pressure vessel design, tension/compression spring design, and welded beam design problems), biomedical real-life problems (breast cancer and heart disease detection), and 14 real-world problems from the 2011 IEEE Congress on Evolutionary Computation. Furthermore, to refine the resulting registration, the iterative closet point (ICP) method [45,46] is used because of its ability to refine registered results [11,34,39]. In the final step, we reconstruct the 3D tooth models.

2. Registration Method

In this section, we will briefly review the 3D registration method used in this paper. The registration between two point cloud images (target ($\mathbf{P} = [p_i]_{M \times 4}$, M is the number of target point cloud points) and source ($\mathbf{Q} = [q_j]_{N \times 4}$, N is the number of source point cloud points) point cloud images) can be found by the following transformation:

$$\mathbf{H}^* = \operatorname{argmin}_{\mathbf{H}} f(\mathbf{H}(\mathbf{Q}), \mathbf{P}) \quad (1)$$

where \mathbf{H} is the geometry transform estimated by finding the nearest neighbor between a set of point pairs (p_j and q_j) [46,47], and $f(\cdot)$ is an objective function (minimum distance error between two corresponding points). Hence, the mean squared error (MSE) can be used as $f(\cdot)$ to find a suitable \mathbf{H}^* as

$$\mathbf{H}^* = \operatorname{argmin}_{\mathbf{H}} \frac{1}{N} \sum_{j=1}^N \left(q_j \cdot \mathbf{H}^T - p_j \right)^2 \quad (2)$$

$$p_j = \operatorname{argmin}_{p_i \in \mathbf{P}} \left\| q_j \cdot \mathbf{H}^T - p_i \right\|. \quad (3)$$

In this case, there are 15 unknown parameters, i.e., 3, 3, 3, and 6 parameters for scaling (\mathbf{S}), translation (\mathbf{T}), rotation (\mathbf{R}), and shearing (\mathbf{SH}), respectively [48]. To give a simpler

equation, let $cox = \cos(\phi_x)$, $coy = \cos(\phi_y)$, $coz = \cos(\phi_z)$, $six = \sin(\phi_x)$, $siy = \sin(\phi_y)$, and $siz = \sin(\phi_z)$; then, the 3D transformation matrix \mathbf{H} is computed as

$$\mathbf{H} = \mathbf{T} \times \mathbf{S} \times \mathbf{R} \times \mathbf{SH}, \quad (4)$$

$$\mathbf{H} = \begin{bmatrix} 1 & 0 & 0 & t_x \\ 0 & 1 & 0 & t_y \\ 0 & 0 & 1 & t_z \\ 0 & 0 & 0 & 1 \end{bmatrix} \begin{bmatrix} s_x & 0 & 0 & 0 \\ 0 & s_y & 0 & 0 \\ 0 & 0 & s_z & 0 \\ 0 & 0 & 0 & 1 \end{bmatrix} \begin{bmatrix} coy \times coz & -coy \times siz & siy & 0 \\ six \times siy \times coz + cox \times siz & -six \times siy \times siz + cox \times coz & -six \times coy & 0 \\ -cox \times siy \times coz + six \times siz & cox \times siy \times siz + six \times coz & cox \times coy & 0 \\ 0 & 0 & 0 & 1 \end{bmatrix} \begin{bmatrix} 1 & sh_1 & sh_2 & 0 \\ sh_3 & 1 & sh_4 & 0 \\ sh_5 & sh_6 & 1 & 0 \\ 0 & 0 & 0 & 1 \end{bmatrix} \quad (5)$$

Hence,

$$\mathbf{H} = \begin{bmatrix} a & d & g & t_x \\ b & e & i & t_y \\ c & f & j & t_z \\ 0 & 0 & 0 & 1 \end{bmatrix}, \quad (6)$$

where

$$\begin{aligned} a &= s_x(coy \times coz) + sh_3s_x(-coy \times siz) + sh_5s_x(siy) \\ b &= s_y(six \times siy \times coz + cox \times siz) + sh_3s_y(-six \times siy \times siz + cox \times coz) + sh_5s_y(-six \times coy) \\ c &= s_z(-cox \times siy \times coz + six \times siz) + sh_3s_z(cox \times siy \times siz + six \times coz) + sh_5s_z(cox \times coy) \\ d &= sh_1s_x(coy \times coz) + s_x(-coy \times siz) + sh_6s_x(siy) \\ e &= sh_1s_y(six \times siy \times coz + cox \times siz) + s_y(-six \times siy \times siz + cox \times coz) + sh_6s_y(-six \times coy) \\ f &= sh_1s_z(-cox \times siy \times coz + six \times siz) + s_z(cox \times siy \times siz + six \times coz) + sh_6s_z(cox \times coy) \\ g &= sh_2s_x(coy \times coz) + sh_4s_x(-coy \times siz) + s_x(siy) \\ i &= sh_2s_y(six \times siy \times coz + cox \times siz) + sh_4s_y(-six \times siy \times siz + cox \times coz) + s_y(-six \times coy) \\ j &= sh_2s_z(-cox \times siy \times coz + six \times siz) + sh_4s_z(cox \times siy \times siz + six \times coz) + s_z(cox \times coy) \end{aligned} \quad (7)$$

It is worthwhile noting that a through j are non-rigid transformations resulting from the combination of scaling, shearing, and rotation properties.

To find the optimal \mathbf{H} , the proposed grey wolf optimization algorithm with behavior considerations and dimensional learning strategies (BCDL-GWO) algorithm described in the following section is utilized. Table 1 shows the defined search space with 15-dimensional individuals in the swarm.

Table 1. Parameters boundaries in optimization process.

Parameters	Lower Bound	Upper Bound
t_x, t_y, t_z	−1.5 (cm)	1.5 (cm)
ϕ_x, ϕ_y, ϕ_z	−45 (deg)	45 (deg)
s_x, s_y, s_z	0.8 (20% downscaling)	1.2 (20% upscaling)
$sh_1, sh_2, sh_3, sh_4, sh_5, sh_6$	−0.5 (cm)	0.5 (cm)

2.1. Overview of Grey Wolf Optimizer Algorithm (GWO)

The gray wolf optimizer (GWO) [40] algorithm is divided into five mathematical models, i.e., (1) social hierarchy, (2) encircling prey, (3) hunting prey, (4) attacking prey (exploitation), and (5) seeking prey (exploration). The wolves are first generated as a set of candidate solutions (search agents) by randomization. At each generation, the wolves, called omega (ω), are guided by their three leaders, named alpha (α), beta (β), and delta (δ), to find more favorable regions in search spaces while searching or hunting for prey. Let $X = \{\mathbf{x}_l | l = 1 \dots K\}$; $\mathbf{x}_l = \{x_{lj} | j = 1 \dots d\}$ be a set of K search agents (individuals) with d -dimensional feature space. The encircling behavior of the l th grey wolf (\mathbf{x}_l) around the p th prey (\mathbf{x}_p) in the j th dimension at iteration (t) is

$$\mathbf{D}_p^t = \left| \mathbf{C}_p^t \cdot \mathbf{x}_p^t - \mathbf{x}_l^t \right| \quad (8)$$

$$\mathbf{x}_l^t = \mathbf{x}_p^t - \mathbf{A}_p^t \cdot \mathbf{D}_p^t \quad (9)$$

where \mathbf{D}_p^t is the distance between \mathbf{x}_l and \mathbf{x}_p at iteration t . The \mathbf{A}_p^t and \mathbf{C}_p^t are defined as

$$\mathbf{A}_p^t = 2 \times \mathbf{a} \cdot \mathbf{r}_1 - \mathbf{a} \quad (10)$$

$$\mathbf{C}_p^t = 2 \times \mathbf{r}_2 \quad (11)$$

where the components of \mathbf{a} decrease linearly from 2 to 0 over the course of iterations. \mathbf{r}_1 and \mathbf{r}_2 are random vectors in $[0, 1]$. Therefore, each element in \mathbf{A}_p^t will be a random value in $[-a, a]$, whereas that in \mathbf{C}_p^t will be a random value in $[0, 2]$. The position update equation of each individual will follow the 3 leaders, i.e., α , β , and δ represented by \mathbf{x}_α^t , \mathbf{x}_β^t , and \mathbf{x}_δ^t , respectively.

$$\mathbf{D}_\alpha^t = |\mathbf{C}_\alpha^t \cdot \mathbf{x}_\alpha^t - \mathbf{x}_l^t|, \mathbf{D}_\beta^t = |\mathbf{C}_\beta^t \cdot \mathbf{x}_\beta^t - \mathbf{x}_l^t|, \text{ and } \mathbf{D}_\delta^t = |\mathbf{C}_\delta^t \cdot \mathbf{x}_\delta^t - \mathbf{x}_l^t| \quad (12)$$

$$\mathbf{x}_1^t = \mathbf{x}_\alpha^t - \mathbf{A}_\alpha^t \cdot \mathbf{D}_\alpha^t, \mathbf{x}_2^t = \mathbf{x}_\beta^t - \mathbf{A}_\beta^t \cdot \mathbf{D}_\beta^t, \text{ and } \mathbf{x}_3^t = \mathbf{x}_\delta^t - \mathbf{A}_\delta^t \cdot \mathbf{D}_\delta^t \quad (13)$$

then

$$\mathbf{x}_l^{t+1} = \frac{\mathbf{x}_1^t + \mathbf{x}_2^t + \mathbf{x}_3^t}{3} \quad (14)$$

2.2. The Modified GWO Algorithm with Behavior Considerations and Dimensional Learning (BCDL-GWO)

The modified GWO with behavior considerations and dimensional learning is based on the idea of [41–44]. Firstly, we incorporate the Sine Cosine Algorithm (SCA) [41] in the alpha grey wolf to alleviate the unbalancing between exploration and exploitation and to help with the premature convergence by

$$\begin{aligned} \mathbf{D}_\alpha^t &= \text{rand}() \times \sin(\text{rand}()) \times |\mathbf{C}_\alpha^t \cdot \mathbf{x}_\alpha^t - \mathbf{x}_l^t|; \text{ if } \text{rand}() < 0.5 \\ \mathbf{D}_\alpha^t &= \text{rand}() \times \cos(\text{rand}()) \times |\mathbf{C}_\alpha^t \cdot \mathbf{x}_\alpha^t - \mathbf{x}_l^t|; \text{ otherwise} \end{aligned} \quad (15)$$

Each j th element of \mathbf{C}_α^t , \mathbf{C}_β^t , and \mathbf{C}_δ^t is modified following the method in [49] as

$$\begin{aligned} \mathbf{C}_{\alpha,j}^t &= 1 + (2 \times r_3 - 1) \times c^2 \\ \mathbf{C}_{\beta,j}^t &= 1 + (2 \times r_4 - 1) \times c^2 \\ \mathbf{C}_{\delta,j}^t &= 1 + (2 \times r_5 - 1) \times c^2 \end{aligned} \quad (16)$$

where r_3 , r_4 , and r_5 are the uniformly distributed random numbers in $[0, 1]$. c is decreasing linearly from 1 to 0 over the course of iterations as follows:

$$c = c_{\max} - (c_{\max} - c_{\min}) \times \left(\frac{t-1}{T-1} \right); c_{\min} = 0, c_{\max} = 1 \quad (17)$$

Therefore, each element in vector \mathbf{C} is stochastically generated in $[0, 2]$ in the first iteration and decreases to 1 at the final iteration. This process helps to provide a better exploration capability. The control vectors \mathbf{A}_α^t , \mathbf{A}_β^t , and \mathbf{A}_δ^t are calculated as in Equation (10) with a calculated by [50]

$$a = 2 \times \left(\frac{T-t}{T} \right)^\mu \quad (18)$$

where T is the total number of iterations, and $0 < \mu \leq 2$.

Our hypothesis is that the alpha grey wolf is the most important leader; hence, the updated position of each omega grey wolf is modified to [51]

$$\mathbf{x}_l^{t+1} = w_1^t \mathbf{x}_1^t + w_2^t \mathbf{x}_2^t + w_3^t \mathbf{x}_3^t; w_1^t + w_2^t + w_3^t = 1 \quad (19)$$

where

$$\begin{aligned} w_1^t &= \cos \theta \\ w_2^t &= 0.5 \sin \theta \cos \varphi \\ w_3^t &= 1 - (w_1^t + w_2^t) \\ \text{with } \theta &= \frac{2}{\pi} \cos^{-1} \left(\frac{1}{3} \right) \tan^{-1}(t), \varphi = 0.5 \tan^{-1}(t) \end{aligned} \quad (20)$$

From Equation (20), $w_1 \geq w_2 \geq w_3$. w_1 is close to 1, and w_2 and w_3 are close to 0 at the beginning. These values will finally be close to 1/3 in the last iteration.

Now, we are ready to incorporate real-life behavioral considerations into the algorithm [52] by discarding the wolves during the migration (prey searching) with low fitness values and allowing mating (crossover and mutation as in the genetic algorithm) to improve the pack's diversity. However, in our GWO, the first half of the iteration is focused on the exploration behavior (when $|A| > 1$), whereas the remaining half is transformed into exploitation behavior (when $|A| < 1$). Hence, we applied the Lévy flights (LF) [42] and Random Opposition Learning (ROL) [43] to improve the pack's diversity and to enhance the capability of the global and local search. The LF is also applied to each element j of the three leaders as

$$\begin{aligned} \mathbf{x}_{1,j}^{levy} &= \left(\mathbf{x}_{\alpha,j}^t - \mathbf{A}_{\alpha,j}^t \times \mathbf{D}_{\alpha,j}^t \right) + levy_{1,j}^t \\ \mathbf{x}_{2,j}^{levy} &= \left(\mathbf{x}_{\beta,j}^t - \mathbf{A}_{\beta,j}^t \times \mathbf{D}_{\beta,j}^t \right) + levy_{2,j}^t \\ \mathbf{x}_{3,j}^{levy} &= \left(\mathbf{x}_{\delta,j}^t - \mathbf{A}_{\delta,j}^t \times \mathbf{D}_{\delta,j}^t \right) + levy_{3,j}^t \end{aligned} \quad (21)$$

The LF is defined as

$$levy_{i,j}^t = \eta_j \times \alpha_j \oplus \frac{u}{|v|^{1/\beta}} \times \left(\mathbf{x}_{i,j}^t - \mathbf{x}_{\alpha,j}^t \right) \quad (22)$$

where

$$\begin{aligned} \eta &\sim N(0, 1), u \sim N(0, \sigma_u^2), v \sim N(0, \sigma_v^2) \\ \sigma_u &= \left\{ \frac{\Gamma(1+\beta) \sin(\pi\beta/2)}{\Gamma[(1+\beta)/2] \beta 2^{(\beta-1)/2}} \right\}^{1/\beta}, \sigma_v = 1 \end{aligned} \quad (23)$$

and Γ is a standard gamma function. In the experiment, we set β to 1.5, and α decreases over time [53] as follows:

$$\alpha_j = \frac{L/10}{\sqrt{t \times d}}; L = (ub_j - lb_j) \quad (24)$$

with lb_j and ub_j are the lower and upper bound, respectively, of the search space in the j th dimension. To add in the ROL in the exploitation behavior [43], suppose $\hat{\mathbf{x}}_l = \{\hat{\mathbf{x}}_{l,j} | j = 1 \dots d\}$; $\hat{\mathbf{x}}_{l,j} \in [lb_j, ub_j]$ be a d -dimensional vector with

$$\hat{\mathbf{x}}_{l,j} = lb_j + ub_j - rand() \times \mathbf{x}_{l,j}^b \quad (25)$$

where \mathbf{x}_l^b is the individual best [54] of the l th grey wolf. Now, we introduce a new candidate solution (\mathbf{x}_l^{BC}) as

$$\mathbf{x}_{l,j}^{BC} = \begin{cases} \left(w_1^t \mathbf{x}_{1,j}^t + w_2^t \mathbf{x}_{2,j}^t + w_3^t \mathbf{x}_{3,j}^t \right) + levy_{l,j}^t, & \text{if } |A| > 1 \text{ \& } rand() \leq 0.5 \\ w_1^t \mathbf{x}_{1,j}^{levy} + w_2^t \mathbf{x}_{2,j}^{levy} + w_3^t \mathbf{x}_{3,j}^{levy}, & \text{if } |A| > 1 \text{ \& } rand() > 0.5 \\ \hat{\mathbf{x}}_{l,j}, & \text{if } |A| \leq 1 \end{cases} \quad (26)$$

It is worth noting that the fitness function in the BCDL-GWO ($f(\cdot)$) is the aforementioned MSE.

The new update position is

$$\mathbf{x}_l^{t+1} = \begin{cases} \mathbf{x}_l^{BC}, & \text{if } f(\mathbf{x}_l^{BC}) < f(\mathbf{x}_l^{t+1}) \\ \mathbf{x}_l^{t+1}, & \text{otherwise} \end{cases} \quad (27)$$

For the dimensional learning part [55], we suppose $\mathbf{x}_l^{DL} = \{\mathbf{x}_{l,j}^{DL} | j = 1 \dots d\}$. The distance between the current and the next position of \mathbf{x}_l^t is

$$R_l^t = \|\mathbf{x}_l^t - \mathbf{x}_l^{t+1}\| \quad (28)$$

The neighborhood of \mathbf{x}_l^t is defined by

$$N_l^t = \{\mathbf{x}_k^t | \mathbf{D}_{lk}^t \leq R_l^t\} \text{ where } \mathbf{D}_{lk}^t = \|\mathbf{x}_l^t - \mathbf{x}_k^t\|, \mathbf{x}_k^t \in K \quad (29)$$

Hence, each j th element of \mathbf{x}_l^{DL} is calculated by

$$\mathbf{x}_{l,j}^{DL} = \mathbf{x}_{l,j}^t + \text{rand}() \times (\mathbf{x}_{n,j}^t - \mathbf{x}_{r,j}^t) \quad (30)$$

where \mathbf{x}_n^t and \mathbf{x}_r^t are randomly selected from N_l^t and search agents, respectively. Then, the updated position will be

$$\mathbf{x}_l^{t+1} = \begin{cases} \mathbf{x}_l^{DL}, & \text{if } f(\mathbf{x}_l^{DL}) < f(\mathbf{x}_l^{t+1}) \\ \mathbf{x}_l^{t+1}, & \text{else} \end{cases} \quad (31)$$

Finally, the position of each grey wolf will only change if the next fitness value is better than the current one. Hence, the final update position equation will be

$$\mathbf{x}_l^{t+1} = \begin{cases} \mathbf{x}_l^{t+1}, & \text{if } f(\mathbf{x}_l^{t+1}) < f(\mathbf{x}_l^t) \\ \mathbf{x}_l^t, & \text{otherwise} \end{cases} \quad (32)$$

The BCDL-GWO algorithm is summarized as shown in Algorithm 1.

The BCDL-GWO optimal solution is selected from the global best in the last population. The iterative closest point algorithm (ICP) method, as in [45,55] with the Nelder–Mead simplex method [56], is utilized to fine-tune the registration results. Table 2 shows the parameters used in our experiment.

Table 2. BCDL-GWO parameters configuration.

Parameters	Symbols	Values
Search agents (wolves)	K	100
Iterations	T	2000
Control parameter a	a_0	2
Control parameter c	c_0	2
Nonlinear exponent indices	μ	0.5, 1.0, 1.5, 2.0
Lévy distribution	β	1.5

Algorithm 1. BCDL-GWO algorithm

Input: K population size, maximum iterations T .
Output: Optimal solution.
Initial: K wolves, $t = 0$.
While $t \leq T$
 Evaluate fitness value $f(\mathbf{x}_l^t)$ for each wolf $\mathbf{x}_l^t \forall l = 1$ to K .
 Find three best leaders, i.e., $\mathbf{x}_\alpha^t, \mathbf{x}_\beta^t, \mathbf{x}_\delta^t$.
 Update individual best positions $\mathbf{x}_l^b \forall l = 1$ to K .
 Update \mathbf{A}_p^t , and \mathbf{C}_p^t using Equations (10) and (11), respectively.
 For each wolf in GWO-SCA procedure
 Update current position \mathbf{x}_l^{t+1} using Equation (19).
 Evaluate fitness $f(\mathbf{x}_l^{t+1})$.
 End For
 For each wolf in behavior considerations procedure
 Generate new candidate solution \mathbf{x}_l^{BC} using Equation (26).
 Evaluate fitness $f(\mathbf{x}_l^{BC})$.
 Update \mathbf{x}_l^{t+1} using Equation (27).
 End For
 For each wolf in dimensional learning procedure
 Generate new candidate solution \mathbf{x}_l^{DL} using equations (30).
 Evaluate fitness $f(\mathbf{x}_l^{DL})$.
 Update \mathbf{x}_l^{t+1} using Equation (31).
 End For
 Update \mathbf{x}_l^{t+1} using Equation (32).
 $t = t + 1$
End While

3. Experimental Results

The diagram of the 3D reconstruction with the optimal transformation matrix \mathbf{H}^{-1} (transform from source point cloud to target point cloud) found by the BCDL-GWO is shown in Figure 1. To fine-tune the resultant \mathbf{H}^{-1} , the ICP method is used. Finally, the 3D tooth models are reconstructed based on the registered source and target point clouds.

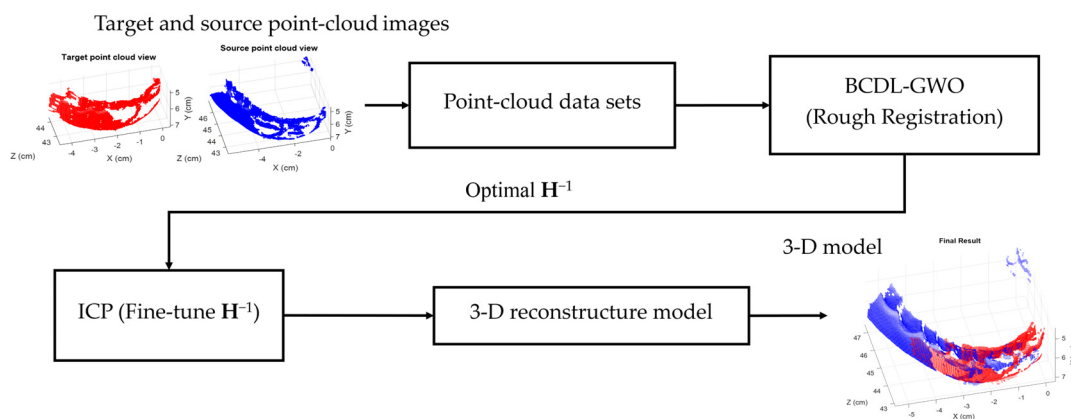


Figure 1. Three-dimensional reconstruction with BCDL-GWO.

We first test our system on synthetic cylindrical and pyramid shapes as shown in Figure 2.

The transformation matrix used to generate from source to target point clouds for both shapes is

$$\mathbf{H} = \begin{bmatrix} 0.882050 & -0.285362 & -0.555884 & -0.061153 \\ 0.225174 & 1.041540 & 0.181496 & 0.063487 \\ 0.249299 & -0.413927 & 0.966936 & -0.163016 \\ 0 & 0 & 0 & 1 \end{bmatrix} \quad (33)$$

Hence, the \mathbf{H}^{-1} that the BCDL-GWO needs to find is

$$\mathbf{H}^{-1} = \begin{bmatrix} 0.901895 & 0.421703 & 0.439339 & 0.1 \\ -0.143742 & 0.826257 & -0.237726 & -0.1 \\ -0.294063 & 0.244980 & 0.819157 & 0.1 \\ 0 & 0 & 0 & 1 \end{bmatrix} \quad (34)$$

We compare the results from the BCDL-GWO with μ varied from 0.5 to 2.0 with a step size of 0.5 with those from our previous work (SR-PSO) [39]. Tables 3 and 4 show the best registration MSEs results using the BCDL-GWO algorithm with and without refining the ICP method on the synthetic cylindrical and pyramid shapes, respectively. The best result on the synthetic cylindrical shape with MSE of 2.71×10^{-27} from BCDL-GWO is at $\mu = 0.5$. Whereas that on the synthetic pyramid shape with MSE of 7.79×10^{-20} is at the same μ . The final best \mathbf{H}^{-1} from both synthetic shapes is the same. Because the MSE is extremely small, both final best \mathbf{H}^{-1} are the same as \mathbf{H}^{-1} shown in Equation (34).

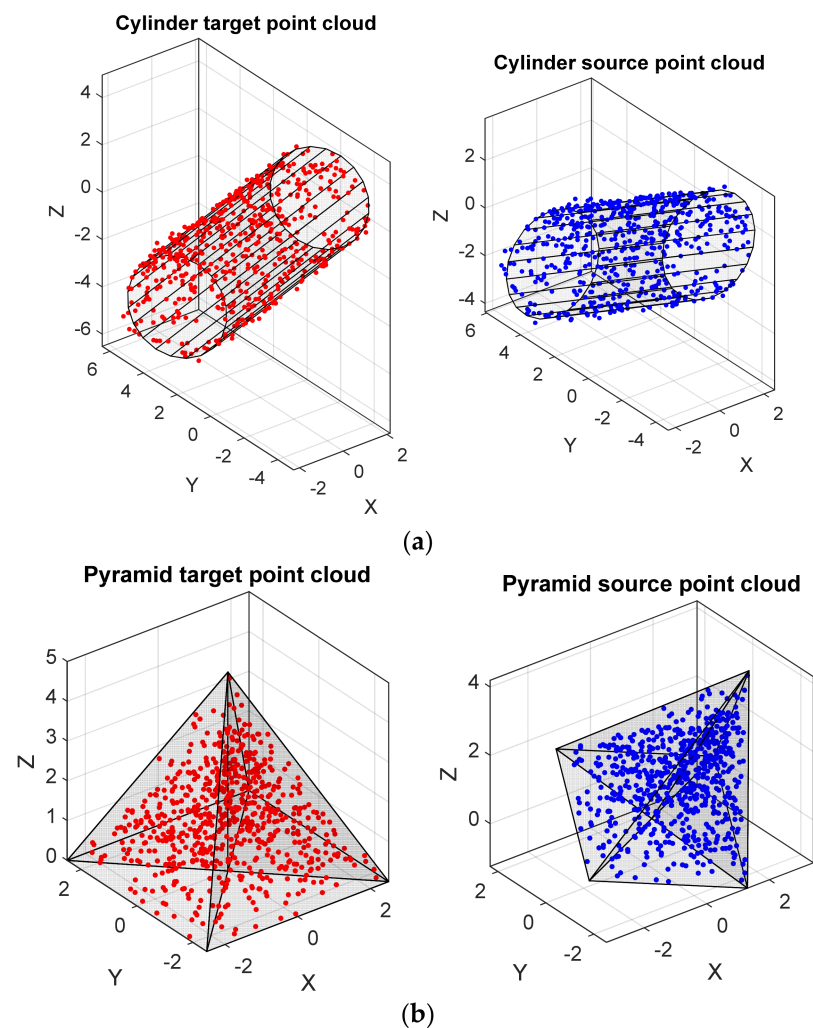


Figure 2. The original shape (target point cloud) and the 3D transformation (source point cloud) of (a) synthetic cylindrical and (b) synthetic pyramid shapes.

The resulting registration of two cylindrical images and two pyramid images are shown in Figure 3a,b, respectively. It can be said that the best result from the BCDL-GWO is comparable with the best one from SR-PSO ($\alpha = 1.5$). And when we look at the results from the BCDL-GWO with the other μ , those are better than that from the SR-PSO with the other α . To confirm this result, we also report the average \pm standard deviation from

several experiments of this algorithm on the same data set shown in Tables 5 and 6 for the synthetic cylindrical and pyramid shapes, respectively.

Table 3. The mean squared error (MSE) in pixels² of the registration on the synthetic cylindrical shape.

Research work in [39]	α			
	$\alpha = 0.5$	$\alpha = 1.0$	$\alpha = 1.5$	$\alpha = 2.0$
Without ICP	7.68×10^{-2}	9.23×10^{-2}	3.22×10^{-31}	9.68×10^{-2}
With ICP	7.68×10^{-2}	9.23×10^{-2}	3.22×10^{-31}	9.68×10^{-2}
BCDL-GWO	μ			
	0.5	1.0	1.5	2.0
Without ICP	1.90×10^{-9}	5.37×10^{-11}	3.46×10^{-13}	3.23×10^{-12}
With ICP	2.71×10^{-27}	7.35×10^{-22}	4.11×10^{-26}	3.41×10^{-21}

Table 4. The mean squared error (MSE) in pixels² of the registration on the synthetic pyramid shape.

SR-PSO [39]	α			
	$\alpha = 0.5$	$\alpha = 1.0$	$\alpha = 1.5$	$\alpha = 2.0$
Without ICP	1.14×10^{-3}	1.18×10^{-4}	5.71×10^{-30}	1.70×10^{-4}
With ICP	1.51×10^{-17}	9.66×10^{-18}	5.71×10^{-30}	6.97×10^{-18}
BCDL-GWO	μ			
	0.5	1.0	1.5	2.0
Without ICP	9.37×10^{-10}	3.40×10^{-10}	1.96×10^{-13}	1.95×10^{-12}
With ICP	7.79×10^{-20}	1.23×10^{-18}	1.63×10^{-17}	6.51×10^{-18}

Table 5. The average registration mean squared error (MSE) \pm standard deviation in pixels² on the synthetic cylindrical shape.

SR-PSO [39]	α			
	$\alpha = 0.5$	$\alpha = 1.0$	$\alpha = 1.5$	$\alpha = 2.0$
Without ICP	5.38×10^{-2} $\pm 3.73 \times 10^{-2}$	4.66×10^{-2} $\pm 4.05 \times 10^{-2}$	3.84×10^{-2} $\pm 4.06 \times 10^{-2}$	5.56×10^{-2} $\pm 3.90 \times 10^{-2}$
With ICP	5.38×10^{-2} $\pm 3.73 \times 10^{-2}$	4.66×10^{-2} $\pm 4.05 \times 10^{-2}$	3.84×10^{-2} $\pm 4.06 \times 10^{-2}$	5.56×10^{-2} $\pm 3.90 \times 10^{-2}$
BCDL-GWO	μ			
	0.5	1.0	1.5	2.0
Without ICP	2.91×10^{-9} $\pm 3.73 \times 10^{-9}$	1.14×10^{-10} $\pm 1.7 \times 10^{-10}$	1.07×10^{-11} $\pm 1.67 \times 10^{-11}$	1.19×10^{-11} $\pm 2.26 \times 10^{-11}$
With ICP	1.68×10^{-19} $\pm 4.48 \times 10^{-19}$	4.26×10^{-22} $\pm 1.03 \times 10^{-21}$	2.64×10^{-19} $\pm 8.31 \times 10^{-19}$	5.69×10^{-20} $\pm 1.17 \times 10^{-19}$

We also compare the results from several experiments of both synthetic data sets shown in Tables 7 and 8 with those achieved by the butterfly optimization algorithm (BOA) [57], Harris hawks optimization (HHO) [58], slime mold algorithm (SMA) [59], and whale optimization algorithm (WOA) [60], whereas each method has the best parameter setting. It can be seen that the result from BCDL-GWO without ICP is better than that from all compared methods with ICP. Hence, we can assume that our BCDL-GWO can escape local minima.

We also provide an indirect registration comparison of our BCDL-GWO with other methods without the utilization of swarm intelligence, i.e., Zhan et al. [33], Li et al. [61], and Du et al. [62], and as shown in Table 9. The results also confirm that our BCDL-GWO provides better results than its counterparts.

Table 6. The average registration mean squared error (MSE) \pm standard deviation in pixels² on the synthetic pyramid shape.

SR-PSO [39]	α			
	$\alpha = 0.5$	$\alpha = 1.0$	$\alpha = 1.5$	$\alpha = 2.0$
Without ICP	1.65×10^{-4} $\pm 3.68 \times 10^{-4}$	4.92×10^{-5} $\pm 1.08 \times 10^{-4}$	1.92×10^{-6} $\pm 6.08 \times 10^{-6}$	1.71×10^{-5} $\pm 5.38 \times 10^{-5}$
With ICP	2.83×10^{-18} $\pm 5.91 \times 10^{-18}$	4.90×10^{-19} $\pm 1.55 \times 10^{-18}$	5.71×10^{-18} $\pm 1.81 \times 10^{-17}$	9.92×10^{-18} $\pm 2.79 \times 10^{-17}$

BCDL-GWO	μ			
	0.5	1.0	1.5	2.0
Without ICP	2.30×10^{-9} $\pm 4.76 \times 10^{-9}$	6.29×10^{-10} $\pm 9.14 \times 10^{-10}$	2.49×10^{-10} $\pm 7.04 \times 10^{-10}$	7.35×10^{-12} $\pm 1.76 \times 10^{-11}$
With ICP	2.15×10^{-16} $\pm 6.56 \times 10^{-16}$	3.79×10^{-18} $\pm 4.78 \times 10^{-18}$	5.79×10^{-18} $\pm 9.57 \times 10^{-18}$	6.93×10^{-19} $\pm 2.05 \times 10^{-18}$

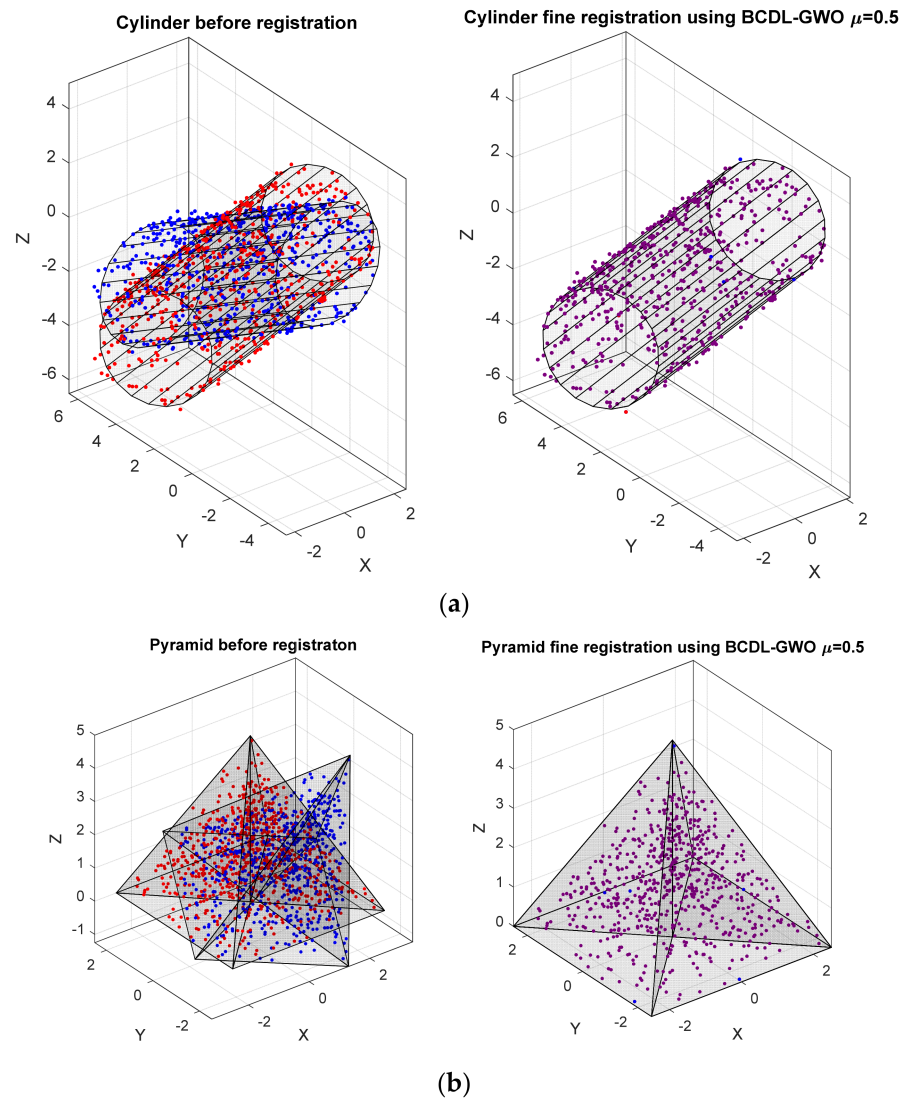


Figure 3. The final best registration using BCDL-GWO with $\mu = 0.5$ of synthetic (a) cylindrical and (b) pyramid images.

Table 7. The best average registration mean squared error (MSE) \pm standard deviation in pixels² on the synthetic cylindrical shapes.

	BOA [57]	HNO [58]	SMA [59]	WOA [60]	SR-PSO [39]	BCDL-GWO
Without ICP	1.08×10^{-1} $\pm 3.83 \times 10^{-3}$	9.63×10^{-2} $\pm 7.49 \times 10^{-3}$	4.78×10^{-2} $\pm 4.70 \times 10^{-2}$	7.27×10^{-2} $\pm 1.99 \times 10^{-2}$	3.84×10^{-2} $\pm 4.06 \times 10^{-2}$	1.07×10^{-11} $\pm 1.67 \times 10^{-11}$
With ICP	8.58×10^{-2} $\pm 1.35 \times 10^{-2}$	8.84×10^{-2} $\pm 1.09 \times 10^{-2}$	4.54×10^{-2} $\pm 4.79 \times 10^{-2}$	6.16×10^{-2} $\pm 3.38 \times 10^{-2}$	3.84×10^{-2} $\pm 4.06 \times 10^{-2}$	4.26×10^{-22} $\pm 1.03 \times 10^{-21}$

Table 8. The best average registration mean squared error (MSE) \pm standard deviation in pixels² on the synthetic pyramid shapes.

	BOA [57]	HNO [58]	SMA [59]	WOA [60]	SR-PSO [39]	BCDL-GWO
Without ICP	4.14×10^{-2} $\pm 2.07 \times 10^{-3}$	4.05×10^{-2} $\pm 8.42 \times 10^{-3}$	7.92×10^{-3} $\pm 6.26 \times 10^{-3}$	3.77×10^{-2} $\pm 8.85 \times 10^{-3}$	1.92×10^{-6} $\pm 6.08 \times 10^{-6}$	7.35×10^{-12} $\pm 1.76 \times 10^{-11}$
With ICP	3.26×10^{-17} $\pm 8.08 \times 10^{-17}$	4.19×10^{-17} $\pm 1.21 \times 10^{-16}$	5.39×10^{-18} $\pm 1.08 \times 10^{-17}$	3.08×10^{-16} $\pm 8.65 \times 10^{-16}$	4.90×10^{-19} $\pm 1.55 \times 10^{-18}$	6.93×10^{-19} $\pm 2.05 \times 10^{-18}$

Table 9. The indirect comparison of several registration data sets with other existing methods.

Data Sets	Objects	Root Mean Squared Error (RMSE)	
		Li et al. [61]	BCDL-GWO
SHOT	Super Mario	4.422×10^{-1}	4.06×10^{-3}
	Doll	4.9×10^{-3}	4.01×10^{-3}
	Duck	5.8×10^{-3}	5.23×10^{-3}
	Frog	4.1×10^{-3}	3.83×10^{-3}
	Peter Rabbit	3.9×10^{-3}	4.05×10^{-3}
	Squirrel	1.29×10^{-2}	3.17×10^{-3}
Stand ford	Bunny Dragon Happy Buddha	Du et al. [62]	
		1.9935×10^{-3}	1.7912×10^{-3}
		1.841×10^{-3}	1.7789×10^{-3}
		2.0950×10^{-3}	2.0279×10^{-3}
Cow and Feet	Cow Feet of man	Mean Squared Error (MSE)	
		Zhan et al. [33]	BCDL-GWO
		1.43×10^{-2}	1.24×10^{-22}
		3.78×10^{-16}	2.13×10^{-18}

From the synthetic data set results, we are certain that the BCDL-GWO can be used in the tooth model 3D reconstruction. The regular tooth model and orthodontic tooth model from [39] were used in the experiment. For each model, six consecutive point cloud coordinate (x, y, z) views with an interval of 30 degrees are used in the experiment. Table 10 shows the information on the tooth point cloud data.

In this experiment, the size of the original image in each view was randomly sampled to 60% with the assumption that there was an overlap between each consecutive view. The voxel hull method [63–65] was used to select representative points inside the overlapping area. After that, the registration process with the parameter setting shown in Table 2 was implemented. Since there were six consecutive views, the hierarchical registration with $F = 6$ was used to increase the registration performance shown in Figure 4. The survival at each level was the best final registration result (BCDL-GWO algorithm with the ICP method), and that result proceeded to the next level of the hierarchical registration.

Table 11 shows the registration MSE results from the BCDL-GWO without the ICP of the regular tooth model at hierarchical level 1, whereas those with ICP are shown in Table 12. Figures 5 and 6 show the best registration of each consecutive pair without and with ICP, respectively.

Table 10. Tooth data set information.

Model	Object View	Object Name	Number of Points
Regular tooth model	1	Img0	28,807
	2	Img1	28,970
	3	Img2	28,983
	4	Img3	25,809
	5	Img4	17,303
	6	Img5	21,739
	Total	Six views	151,592
Orthodontic tooth model	1	Img0	25,301
	2	Img1	25,772
	3	Img2	22,432
	4	Img3	17,167
	5	Img4	22,537
	6	Img5	24,148
	Total	Six views	137,357

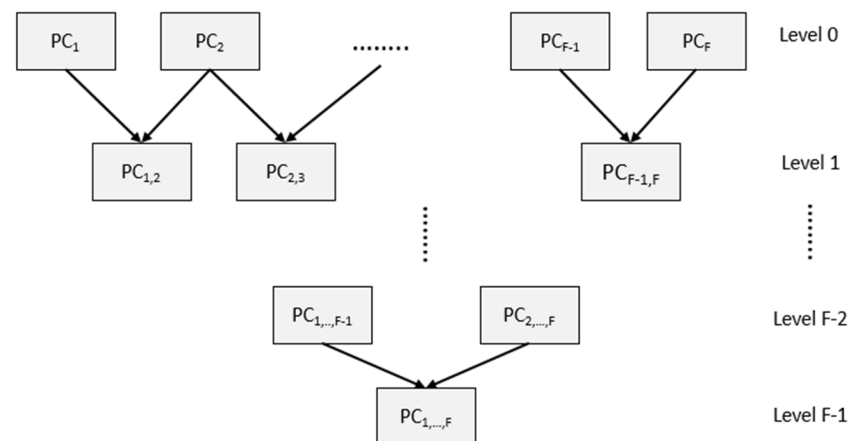


Figure 4. Hierarchical structure for multiple-views registration.

Table 11. MSE of BCDL-GWO on the regular tooth model at hierarchical level 1.

View Pairs	MSE in Micrometer ²			
	$\mu = 0.5$	$\mu = 1.0$	$\mu = 1.5$	$\mu = 2.0$
1 vs. 2	5.8775	6.7106	5.8122	5.8169
2 vs. 3	5.0568	4.9923	4.9406	4.9582
3 vs. 4	5.3752	5.4111	5.4080	5.3940
4 vs. 5	5.5786	5.5135	5.5601	5.4953
5 vs. 6	5.9304	5.7735	5.7640	5.7808

Table 12. MSE of the BCDL-GWO with ICP on the regular tooth model at hierarchical level 1.

View Pairs	MSE in Micrometer ²			
	$\mu = 0.5$	$\mu = 1.0$	$\mu = 1.5$	$\mu = 2.0$
1 vs. 2	5.7533	5.7531	5.7327	5.7328
2 vs. 3	4.9278	4.9266	4.9291	4.9265
3 vs. 4	5.3558	5.3564	5.3854	5.3566
4 vs. 5	5.3860	5.3289	5.3320	5.3412
5 vs. 6	5.7269	5.7316	5.7331	5.7287

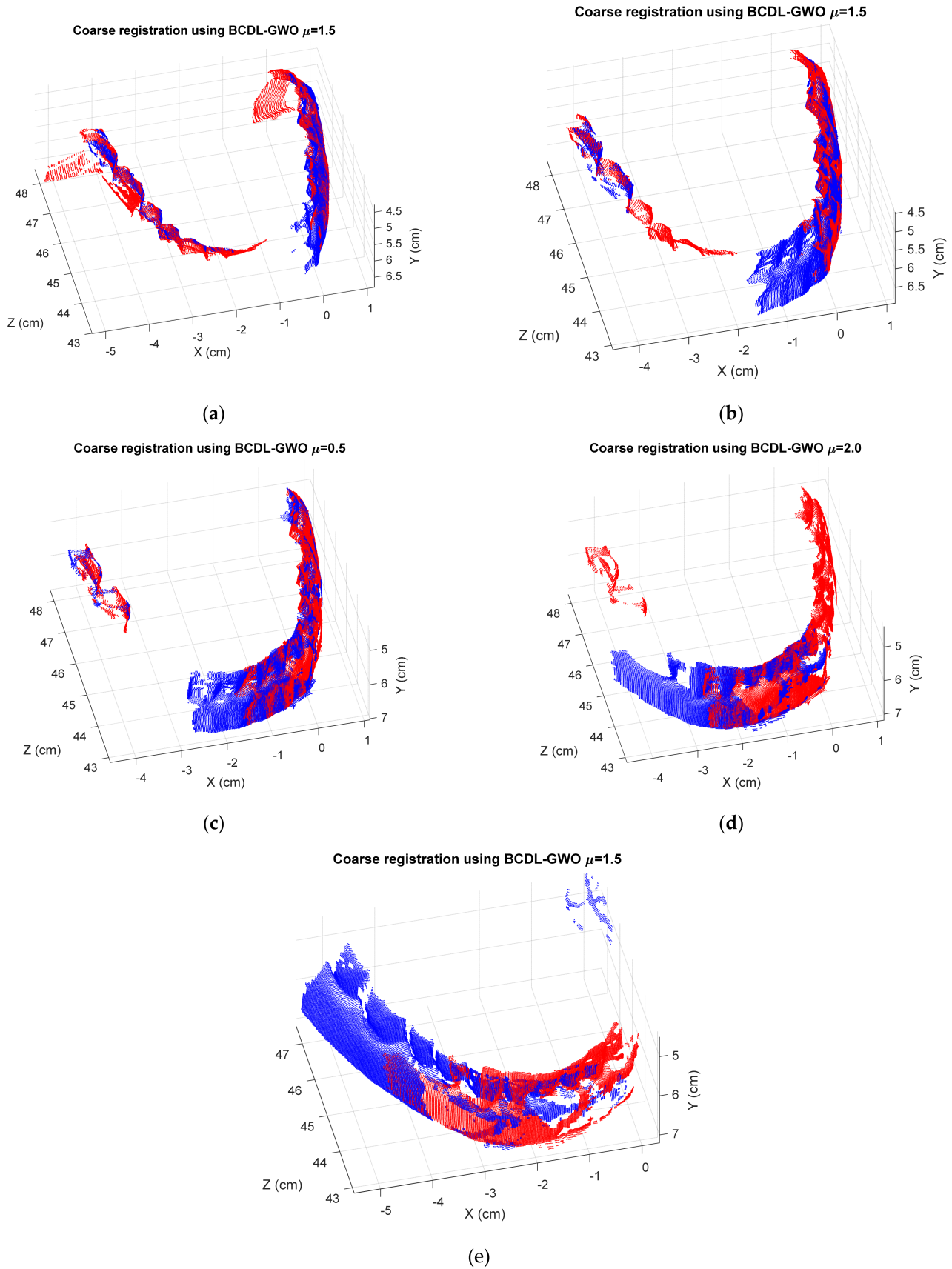


Figure 5. The best registration results of BCDL-GWO only for the following pairs: (a) 1 and 2; (b) 2 and 3; (c) 3 and 4; (d) 4 and 5; (e) 5 and 6.

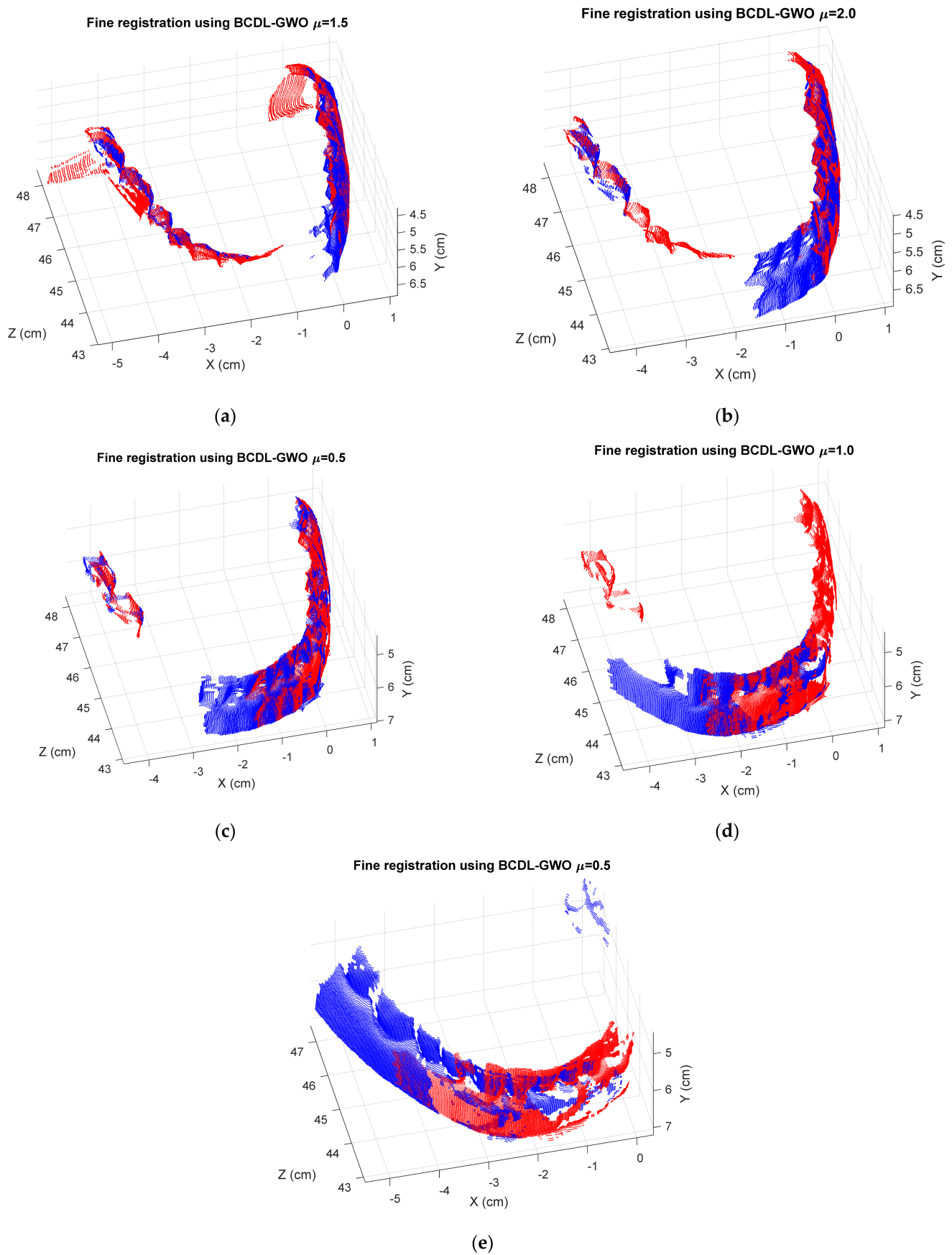


Figure 6. The best registration results of BCDL-GWO with ICP for the following pairs: (a) 1 and 2; (b) 2 and 3; (c) 3 and 4; (d) 4 and 5; (e) 5 and 6.

We compare our results with those from SR-PSO [39] as well. The MSEs of the regular tooth model at hierarchical level 1 are shown in Table 13. From the results, we can see that both methods provide comparable results. However, when we look at the MSEs of the final 3D reconstruction of the regular tooth model from six consecutive views shown in Table 14, we can see that the results from the best BCDL-GWO with ICP ($7.2186 \mu\text{m}^2$ when $\mu = 0.5$) are better than SR-PSO with ICP ($7.3666 \mu\text{m}^2$).

Table 13. MSE comparison on regular tooth model at level 1.

View Pairs	MSE in Micrometer ²			
	Coarse Registration		Fine Registration	
	SR-PSO	BCDL-GWO	SR-PSO	BCDL-GWO
1 vs. 2	5.9300	5.8122	5.8628	5.7327
2 vs. 3	4.8937	4.9406	4.8860	4.9265
3 vs. 4	5.4310	5.3752	5.4017	5.3558
4 vs. 5	5.2666	5.4953	5.1253	5.3289
5 vs. 6	5.8166	5.7640	5.6828	5.7269

Table 14. MSE of the final registration of six consecutive views (μm^2) for the regular tooth model (the best value is in bold).

SR-PSO with ICP		BCDL-GWO with ICP		
$\alpha = 1.5$	$\mu = 0.5$	$\mu = 1.0$	$\mu = 1.5$	$\mu = 2.0$
7.3666	7.2186	7.2188	7.2209	7.2189

The final registration of the regular tooth model is shown in Figure 7. We can see that the reconstruction result provides a good visualization.

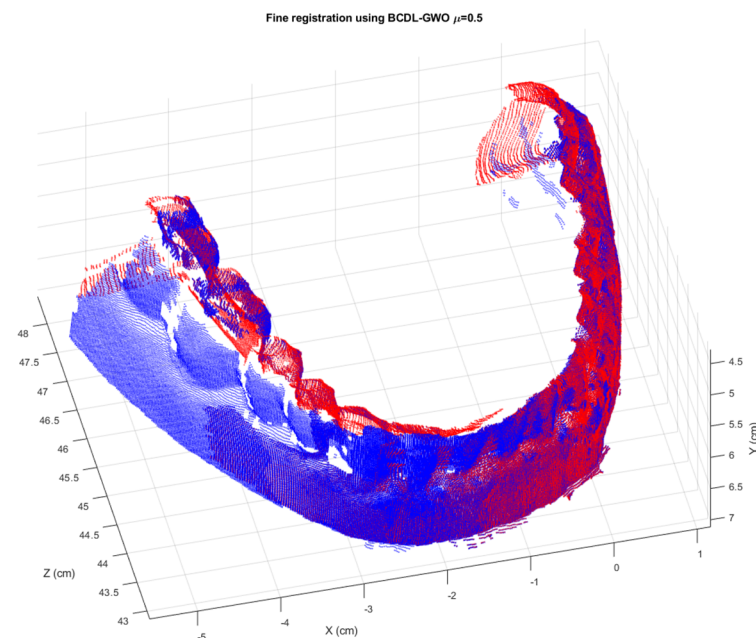


Figure 7. The final registration result of six consecutive views of the regular tooth model from the BCDL-GWO with the ICP.

Finally, we implement the BCDL-GWO on the orthodontic tooth model to observe more experiments. The MSE registration results at hierarchical level 1 from the BCDL-GWO and BCDL-GWO with the ICP are shown in Tables 15 and 16, respectively. Figures 8 and 9 show the best registration results for each consecutive pair.

Table 15. MSE of BCDL-GWO on the orthodontic tooth model at hierarchical level 1.

View pairs	MSE in Micrometer ²			
	$\mu = 0.5$	$\mu = 1.0$	$\mu = 1.5$	$\mu = 2.0$
1 vs. 2	5.5267	5.5227	5.6627	5.5413
2 vs. 3	6.2508	6.8335	6.2865	6.1815
3 vs. 4	5.5515	5.3939	5.6002	5.5869
4 vs. 5	6.4284	6.6458	6.4830	6.4737
5 vs. 6	6.1203	5.3183	5.4125	5.3231

Table 16. MSE of BCDL-GWO with ICP on the orthodontic tooth model at hierarchical level 1.

View Pairs	MSE in Micrometer ²			
	$\mu = 0.5$	$\mu = 1.0$	$\mu = 1.5$	$\mu = 2.0$
1 vs. 2	5.5104	5.5089	5.5108	5.5147
2 vs. 3	6.1425	6.1422	6.1423	6.1422
3 vs. 4	5.2838	5.2842	5.2842	5.2720
4 vs. 5	6.3988	6.3931	6.4010	6.4010
5 vs. 6	5.2861	5.2863	5.2804	5.2820

Again, we compare our MSEs on the registration results with those from the SR-PSO, as shown in Table 17. We can see that our proposed algorithm without the ICP method provides better registration results than the SR-PSO without the ICP method, except for a pair of 2 vs. 3. However, for the fine registration, our BCDL-GWO with ICP is comparable with those from the SR-PSO with ICP. But when we look at the final registration 3D orthodontic reconstruction model, as shown in Table 18, the results from the BCDL-GWO with ICP are better than the best results from the SR-PSO with ICP ($7.4130 \mu\text{m}^2$). While the best result from the BCDL-GWO with ICP at $\mu = 1.5$ is $7.3999 \mu\text{m}^2$. The final 3D reconstruction of the orthodontic tooth model is shown in Figure 10. We can see that the reconstruction result can still provide a good visualization.

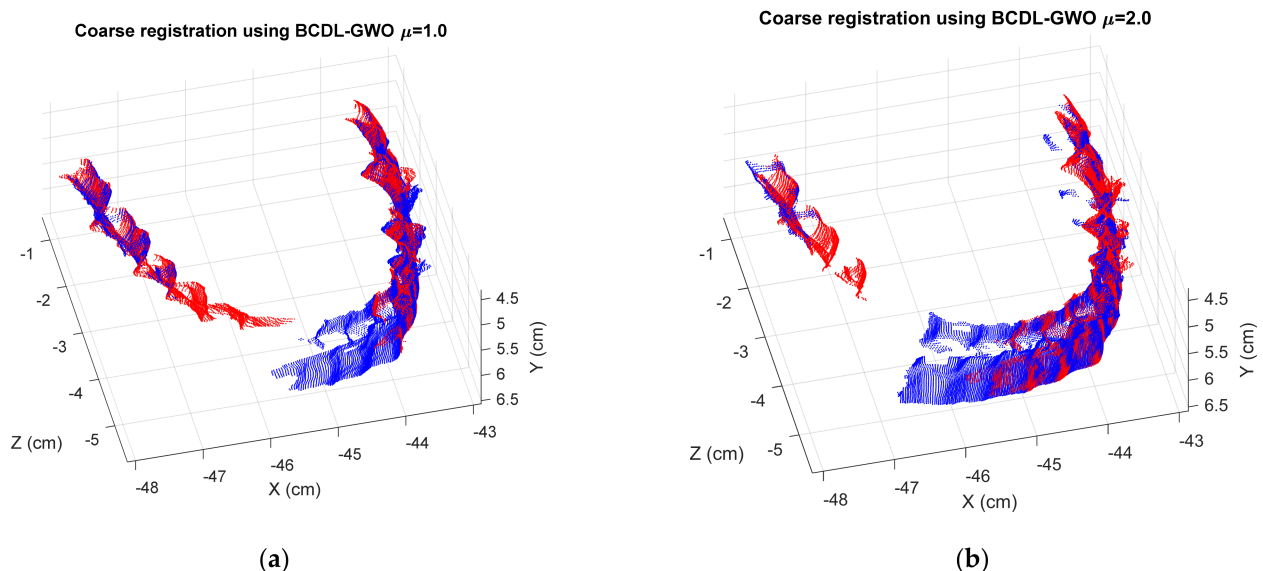


Figure 8. Cont.

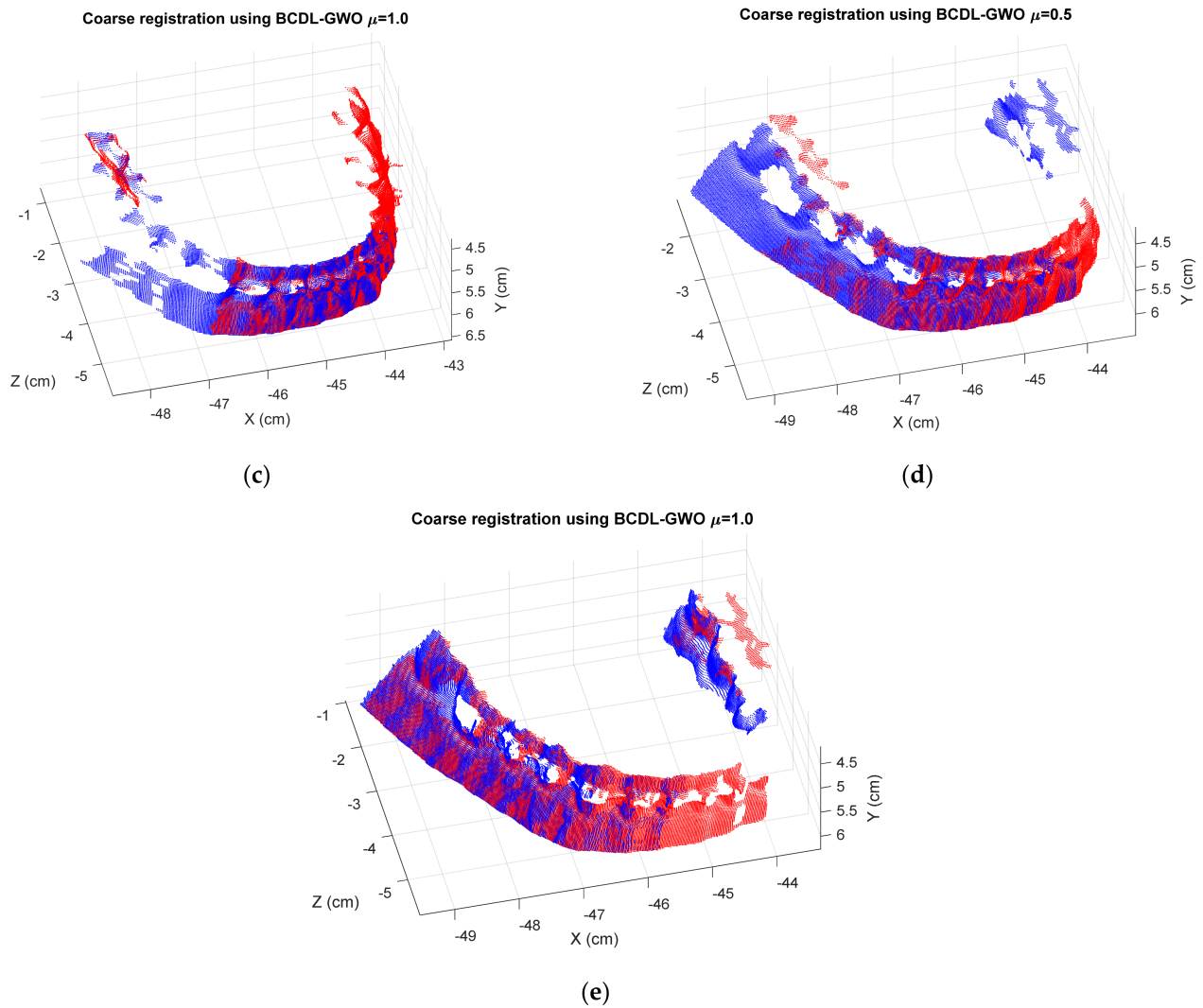


Figure 8. The best registration results of BCDL-GWO for the following pairs: (a) 1 and 2; (b) 2 and 3; (c) 3 and 4; (d) 4 and 5; (e) 5 and 6.

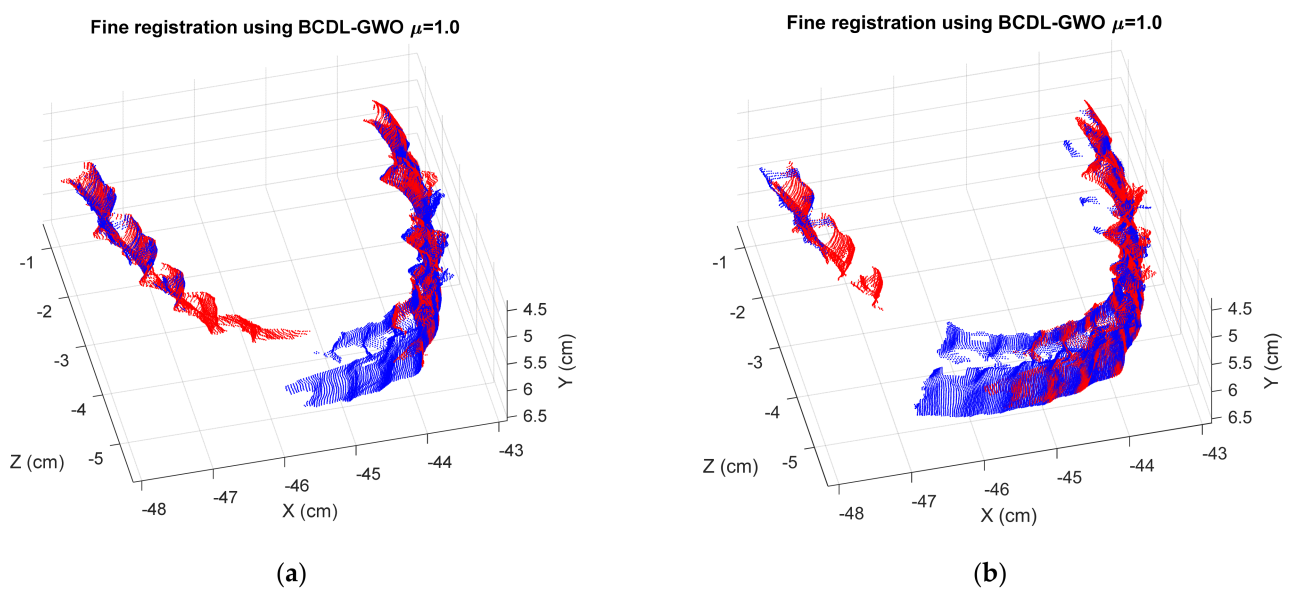


Figure 9. Cont.

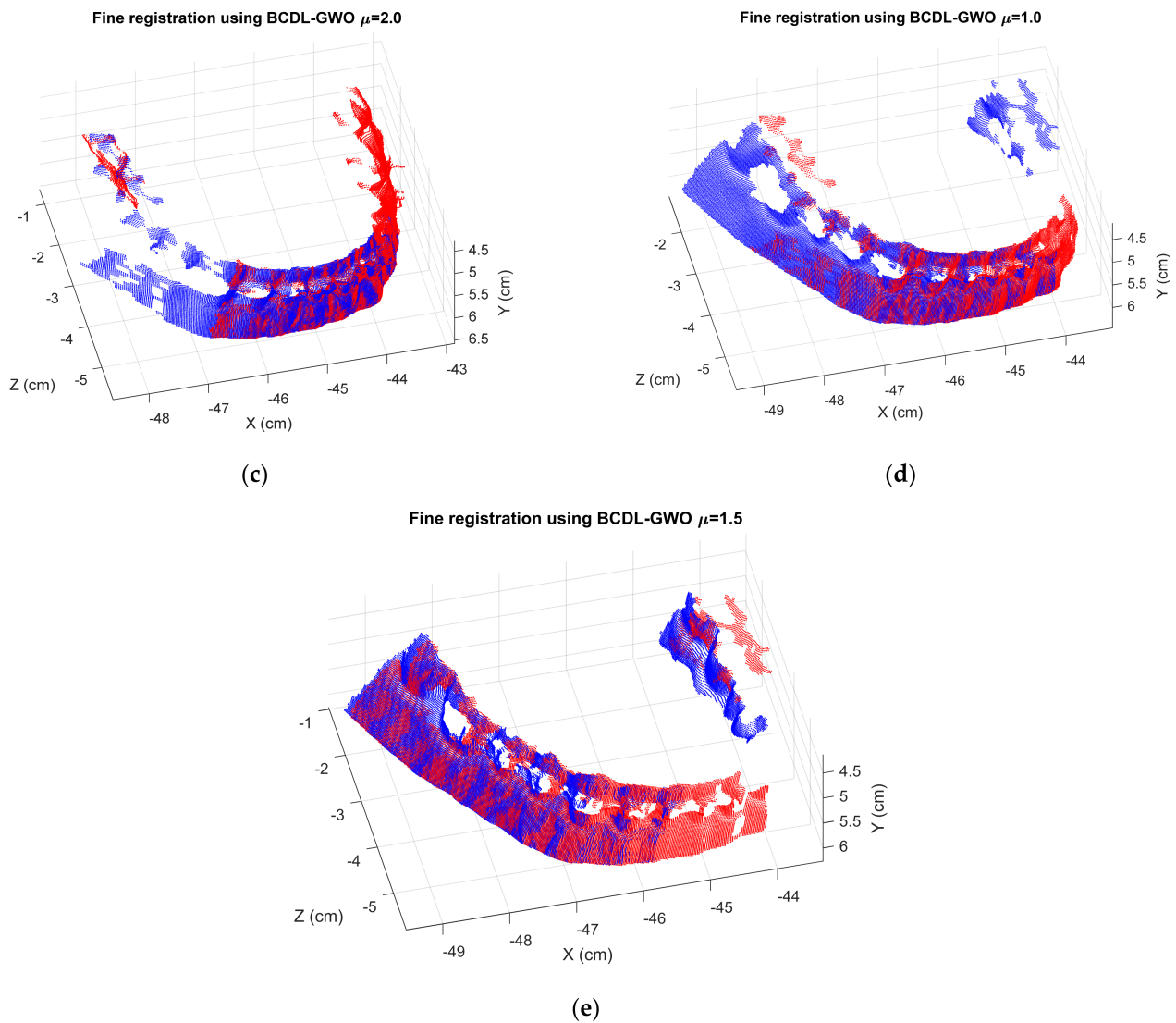


Figure 9. The best registration results of BCDL-GWO with ICP for the following pairs: (a) 1 and 2; (b) 2 and 3; (c) 3 and 4; (d) 4 and 5; (e) 5 and 6.

Table 17. MSE comparison on orthodontic tooth model at hierarchical level 1.

View Pairs	MSE in Micrometer ²			
	Coarse Registration		Fine Registration	
	SR-PSO	BCDL-GWO	SR-PSO	BCDL-GWO
1 vs. 2	5.5553	5.5227	5.5093	5.5089
2 vs. 3	6.1613	6.1815	6.1440	6.1422
3 vs. 4	5.4687	5.3939	5.2706	5.2720
4 vs. 5	6.5847	6.4284	6.3945	6.3931
5 vs. 6	5.3262	5.3183	5.2801	5.2804

Table 18. MSE of the final registration of six consecutive views (micrometer²) for the orthodontic-tooth model (the best value is in bold).

SR-PSO with ICP		BCDL-GWO with ICP		
$\alpha = 0.5$	$\mu = 0.5$	$\mu = 1.0$	$\mu = 1.5$	$\mu = 2.0$
7.4130	7.4000	7.4008	7.3999	7.4001

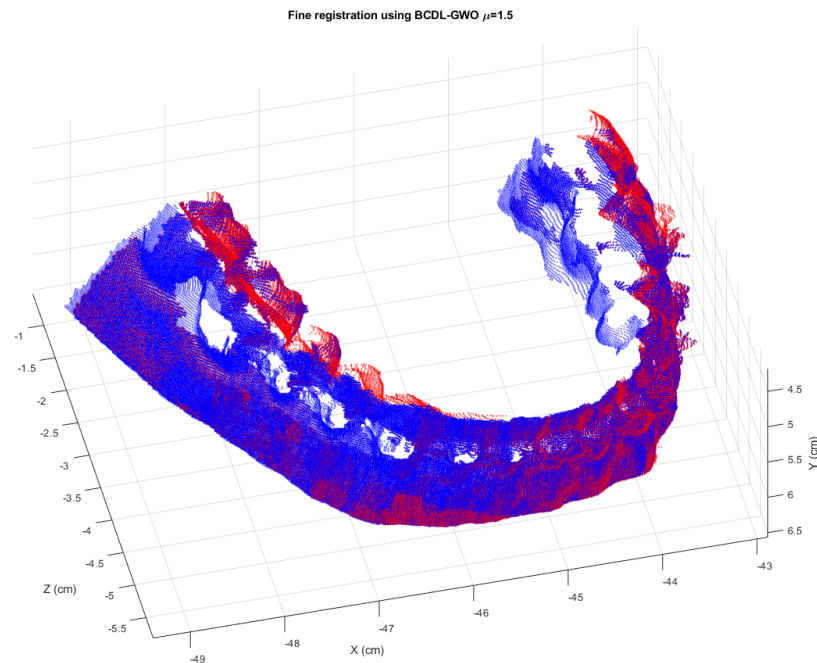


Figure 10. The final registration result of six consecutive views of the orthodontic tooth model from the BCDL-GWO with the ICP.

To confirm that our method is good enough, we indirectly compare our results with those existing methods in the literature on the dental 3D registration data sets. However, those methods were performed on different data sets. The comparison results are shown in Table 19. Again, the results from our BCDL-GWO are better.

Table 19. Indirect comparison results on dental 3D registration data sets.

Research Works	Methods	Objective Functions	Data Sets	Transformations	Registration Errors
Kalla et al. [66]	Downhill simplex method and deformation techniques	Matt's Mutual Information (MMI)	CT images	Non-Rigid	Pre-registered: 0.546 ± 0.233 Elastic-registered: 0.666 ± 0.286 Data set 1: 1.39 ± 2.67 mm
Kim et al. [67]	2D CNN and ICP	Curvature variance of neighbor (CVN)	CT images and 3D scanned models	Rigid	Data set 2: 2.37 ± 3.43 mm Data set 3: 1.01 ± 2.10 mm
Kurniawan et al. [68]	ICP	Root Mean Squared Error (RMSE)	3D point clouds	Rigid	Experiment 1: 0.182 ± 0.032 mm Experiment 2: 0.187 ± 0.041 mm
Chung et al. [69]	CNN and Downhill simplex method	Clustered similarity	CT images and 3D scanned models	Rigid	Surface-based error: 5.11 ± 2.54 mm Landmark-based error: 1.80 ± 0.84 mm
Our proposed method	BCDL-GWO and ICP	Mean Squared Error (MSE)	3D point clouds	Non-Rigid	Tooth model 1: 7.22×10^{-3} mm Tooth model 2: 7.39×10^{-3} mm

One might wonder what the computational complexity of BCDL-GWO is compared with the SR-PSO, BOA, HHO, SMA, and WOA shown in Table 20. To compute the complexity of the BCDL-GWO, we start with the population initialization step. Since there are

K grey wolves in the population and each grey wolf is represented by a D -dimensional vector, the computational complexity in this step is $O(K \times D)$. For the control parameter step, the first operation is the GWO-SCA, which needs $O(K \times D)$. The next operation in this step is Equation (15), which will need $O(D)$. Then, both the position update and fitness evaluation will need $O(K \times D)$. Hence, in this step, it is $O(K \times D)$. However, in the fitness comparison step, it will need $O(K)$. The next step is the behavior consideration procedure. In this step, the new candidate solution calculation from Equation (26) will need $O(K \times D)$. The fitness calculation in this step will need $O(K \times D)$. The update position using Equation (27) will be $O(K \times D)$. Hence, in this step, the complexity will be $O(K \times D)$. Finally, in the dimensional learning procedure step, the distance calculation will need $O(K \times D)$. Equation (29) used in the search agents will need $O(K \times D^2)$. Again, the position update needs $O(K \times D)$. However, in this step, the total complexity is $O(K \times D^2)$. Since there are T iterations, the total complexity of the BCDL-GWO will be $O(T \times K \times D^2)$. For other algorithms, the complexities are calculated similarly. Table 20 shows the Big O of each step in each algorithm. The complexities of all algorithms are very similar. Even though the BCDL-GWO has a slightly higher complexity than the others, the tradeoff with the performance of our BCDL-GWO is still good.

Table 20. Computational time complexities of BCDL-GWO and SR-PSO.

Process	Time Complexities					
	BCDL-GWO	SR-PSO [39]	BOA [57]	HHO [58]	SMA [59]	WOA [60]
Initialization	$O(K \times D)$ *	$O(K \times D)$	$O(K \times D)$	$O(K \times D)$	$O(K \times D)$	$O(K \times D)$
Control parameter calculations	$O(K \times D)$	$O(K \times D)$	$O(K)$	$O(K)$	$O(K \times D)$	$O(K \times D)$
Position update steps	$O(K \times D)$	$O(K \times D)$	$O(K \times D)$	$O(K \times D)$	$O(K \times D)$	$O(K \times D)$
New candidate generation steps	$O(K \times D^2)$	$O(K \times D)$	-	-	-	-
Fitness evaluations	$O(K \times D)$	$O(K \times D)$	$O(K \times D)$	$O(K \times D)$	$O(K \times D)$	$O(K \times D)$
Fitness comparisons	$O(K)$	$O(K)$	$O(K)$	$O(K)$	$O(K \log K)$	$O(K)$

* K denotes population size, and D indicates the number of dimensions in search spaces.

4. Conclusions

To help in dental diagnostic and treatment planning in rural areas with limited access to sophisticated devices, a 3D reconstruction from multi-view optical images is needed. To provide a good 3D reconstruction, a good 3D registration process is required. In this paper, we developed the grey wolf optimization algorithm with behavior considerations and dimensional learning strategies (BCDL-GWO) with iterative closet point (ICP) to find the optimal affine transform in the 3D registration process. We compare the results with those from the statistical randomization-based particle swarm optimization (SR-PSO). We found that the final best result of BCDL-GWO with the ICP yields a mean squared error (MSE) of $7.2186 \mu\text{m}^2$ for 3D reconstruction from six consecutive views of the regular tooth model, whereas that of SR-PSO with the ICP method is $7.3666 \mu\text{m}^2$. The MSE of the BCDL-GWO with the ICP method is $7.3999 \mu\text{m}^2$ for the orthodontic tooth model, while the SR-PSO with the ICP provides $7.4130 \mu\text{m}^2$. We can say that the 3D reconstruction of the regular and orthodontic tooth models from the BCDL-GWO with ICP is better than the SR-PSO with ICP.

We also estimate the computational complexity of both the BCDL-GWO and the SR-PSO. We could say that they are comparable. However, from the nature of the BCDL-GWO, we can also say that it can cope with a premature convergence, an unbalance between exploration and exploitation, and finally, it increases a pack's diversity.

Currently, there is only one research work involving the 3D model to assess dental caries [70]. This shows that there is a need for a 3D model for dental caries assessment.

Hence, in future work, we plan to implement our algorithm in order to simulate dental caries for tooth defections in real situations.

Author Contributions: All authors conceived and designed the experiments; R.W. performed the experiments; and all authors contributed to the writing of the paper. All authors have read and agreed to the published version of the manuscript.

Funding: This research was funded by the Royal Golden Jubilee Ph.D. Program (Grant No. PHD-0170-2558).

Institutional Review Board Statement: Not applicable.

Informed Consent Statement: Not applicable.

Data Availability Statement: No new data were created or analyzed in this study. Data sharing is not applicable to this article.

Acknowledgments: The authors would like to thank the Royal Golden Jubilee Ph.D. Program (RGJ-PhD) for support under grant No. PHD-0170-2558 for financial funding.

Conflicts of Interest: The authors of the paper do not have any conflicts of interest with any companies or institutions. This work was supported by the Thailand Research Fund under the Royal Golden Jubilee Ph.D. Program (Grant No. PHD-0170-2558). This article does not contain any studies with human participants or animals performed by any of the authors.

References

1. Sivakumar, A.; Thangaswamy, V.; Ravi, V. Treatment planning in conservative dentistry. *J. Pharm. Bioallied Sci.* **2012**, *4* (Suppl. S2), S406–S409. [[CrossRef](#)] [[PubMed](#)]
2. Stefanac, S.; Nesbit, S. *Diagnosis and Treatment Planning in Dentistry*, 3rd ed.; Elsevier: Amsterdam, The Netherlands, 2017; ISBN 9780323287302.
3. Hugar, S.M.; Sogi, H.P.S.; Nalawade, T.M.; Sinha, A.; Hugar, S.; Mallikarjuna, R.M. Knowledge, attitude, and practices of oral health care in prevention of early childhood caries among parents of children in Belagavi city: A Questionnaire study. *J. Fam. Med. Prim. Care* **2016**, *5*, 286–290. [[CrossRef](#)] [[PubMed](#)]
4. Yanagisawa, R.; Sugaya, Y.; Kasahara, S.; Omachi, S. Tooth shape reconstruction from dental CT images with the region-growing method. *Dentomaxillofacial Radiol.* **2014**, *43*, 20140080. [[CrossRef](#)]
5. Zhou, X.; Gan, Y.; Xiong, J.; Zhang, D.; Zhao, Q.; Xia, Z. A Method for Tooth Model Reconstruction Based on Integration of Multimodal Images. *J. Healthc. Eng.* **2018**, *2018*, 4950131. [[CrossRef](#)]
6. Zhang, D.; Gan, Y.; Xiong, J.; Xia, Z. Three-dimensional tooth model reconstruction based on fusion of dental computed tomography images and laser-scanned images (Chinese Article). *Shengwu Yixue Gongchengxue Zazhi* **2017**, *34*, 7–14. (In Chinese)
7. Yau, H.-T.; Yang, T.-J.; Chen, Y.-C. Tooth model reconstruction based upon data fusion for orthodontic treatment simulation. *Comput. Biol. Med.* **2014**, *48*, 8–16. [[CrossRef](#)] [[PubMed](#)]
8. Martorelli, M.; Ausiello, P. A novel approach for a complete 3D tooth reconstruction using only 3D crown data. *Int. J. Interact. Des. Manuf.* **2013**, *7*, 125–133. [[CrossRef](#)]
9. Gan, Y.; Tan, J.; Zhao, Q.; Xia, Z. Automatic 3D Tooth Model Reconstruction from CT Images. In Proceedings of the 2014 International Association for Dental Research/Asia Pacific Region (IADR/APR), Cape Town, South Africa, 25 June 2014.
10. Srisilapanan, P.; Nirunsittirat, A.; Roseman, J. Trends over Time in Dental Caries status in Urban and Rural Thai Children. *J. Clin. Exp. Dent.* **2017**, *9*, e1201–e1206. [[CrossRef](#)]
11. Abdel-Basset, M.; Fakhry, A.E.; El-henawy, I.; Qiu, T.; Sangaiah, A.K. Feature and Intensity Based Medical Image Registration Using Particle Swarm Optimization. *J. Med. Syst.* **2017**, *41*, 197. [[CrossRef](#)]
12. Sarvamangala, D.R.; Kulkarni, R.V. Swarm Intelligence Algorithms for Medical Image Registration: A Comparative Study. *Commun. Comput. Inf. Sci.* **2017**, *776*, 451–465. [[CrossRef](#)]
13. Khan, M.K.; Nystrom, I. A Modified Particle Swarm Optimization Applied in Image Registration. In Proceedings of the 2010 20th International Conference on Pattern Recognition, Istanbul, Turkey, 23–26 August 2010; IEEE: Piscataway Township, NJ, USA, 2010; pp. 2302–2305.
14. Jara, R.I.; Buchelly, F.J.; Meschino, G.; Ballarin, V.L. Improved Particle Swarm Optimization algorithm applied to rigid registration in medical images. In Proceedings of the VII Latin American Congress on Biomedical Engineering CLAIB 2016, Bucaramanga, Santander, Colombia, 26–28 October 2016; IFMBE Proceedings. Torres, I., Bustamante, J., Sierra, D., Eds.; Springer: Singapore, 2016; Volume 60, pp. 161–164.
15. Yonghong, Y.; Jiying, L.; Qiang, W.; Tao, Z. Improved Particle Swarm Optimization Image Registration Based on Mutual Information. In Proceedings of the 2019 11th International Conference on Measuring Technology and Mechatronics Automation (ICMTMA), Qiqihar, China, 28–29 April 2019; IEEE: Piscataway Township, NJ, USA, 2019; pp. 450–453.

16. Ramirez, L.; Durdle, N.G.; Raso, V.J. A Parameters Selection Scheme for Medical Image Registration. In Proceedings of the Annual Meeting of the North American Fuzzy Information Processing Society (NAFIPS), Montreal, QC, Canada, 3–6 June 2006; pp. 505–510.
17. Sabuncu, M.R.; Ramadge, P.J. Spatial Information in Entropy-Based Image Registration. In *WBIR 2003, Lecture Notes in Computer Science*; Gee, J.C., Maintz, J.B.A., Vannier, M.W., Eds.; Springer: Berlin/Heidelberg, Germany, 2003; Volume 2717. [\[CrossRef\]](#)
18. Kaur, A.; Kaur, L.; Gupta, S. Image Recognition using Coefficient of Correlation and Structural Similarity Index in Uncontrolled Environment. *Int. J. Comput. Appl.* **2012**, *59*, 32–39. [\[CrossRef\]](#)
19. Daniel, E.; Anitha, J.; Kamaleshwaran, K.K.; Rani, I. Optimum spectrum mask based medical image fusion using Grey Wolf Optimization. *Biomed. Signal Process. Control* **2017**, *34*, 36–43. [\[CrossRef\]](#)
20. Dida, H.; Charif, F.; Benchabane, A. Grey Wolf Optimizer for Multimodal Medical Image Registration. In Proceedings of the Fourth International Conference on Intelligent Computing in Data Sciences (ICDS), Fez, Morocco, 21–23 October 2020; pp. 1–5. [\[CrossRef\]](#)
21. Chakraborty, S.; Pradhan, R.; Ashour, A.S.; Moraru, L.; Dey, N. Grey-Wolf-Based Wang’s Demons for Retinal Image Registration. *Entropy* **2020**, *22*, 659. [\[CrossRef\]](#)
22. Shaw, K.; Pandey, P.; Das, S.; Ghosh, D.; Malakar, P.; Dhabal, S. Image Registration using Bio-inspired Algorithms. In Proceedings of the 2020 IEEE 1st International Conference for Convergence in Engineering (ICCE), Kolkata, India, 5–6 September 2020; pp. 330–334. [\[CrossRef\]](#)
23. Yan, X.; Zhang, Y.; Zhang, D.; Hou, N. Multimodal image registration using histogram of oriented gradient distance and data-driven grey wolf optimizer. *Neurocomputing* **2020**, *392*, 108–120. [\[CrossRef\]](#)
24. Lazar, D.; Jokic, A.; Petrovic, M.; Miljković, Z. Biologically Inspired Optimization Methods for Image Registration in Visual Servoing of a Mobile Robot. In Proceedings of the 7th International Conference on Electrical, Electronic and Computing Engineering (IcETRAN), Etno-Selo Stanišići, Republika Srpska, 28–30 September 2020.
25. Kaur, K.; Budhiraja, S.; Sharma, N. Multimodal Medical Image Fusion based on Gray Wolf Optimization and Hilbert Transform. *Biomed. Pharmacol. J.* **2019**, *12*, 2091–2098. [\[CrossRef\]](#)
26. Dida, H.; Charif, F.; Benchabane, A. Registration of computed tomography images of a lung infected with COVID-19 based in the new meta-heuristic algorithm HPSGWO. *Multimed. Tools Appl.* **2022**, *81*, 18955–18976. [\[CrossRef\]](#)
27. Wachowiak, M.P.; Smolíková, R.; Zheng, Y.; Zurada, J.M.; Elmaghraby, A.S. An Approach to Multimodal Biomedical Image Registration Utilizing Particle Swarm Optimization. *IEEE Trans. Evol. Comput.* **2004**, *8*, 289–301. [\[CrossRef\]](#)
28. Chen, Y.-W.; Mimori, A. Hybrid Particle Swarm Optimization for Medical Image Registration. In Proceedings of the 2009 Fifth International Conference on Natural Computation, Tianjin, China, 14–16 August 2009; IEEE: Piscataway Township, NJ, USA, 2009; Volume 6, pp. 26–30.
29. Abduo, J.; Bennamoun, M. Three-dimensional image registration as a tool for forensic odontology: A preliminary investigation. *Am. J. Forensic Med. Pathol.* **2013**, *34*, 260–266. [\[CrossRef\]](#) [\[PubMed\]](#)
30. Wu, C.; Bradley, D.; Garrido, P.; Zollhöfer, M.; Theobalt, C.; Gross, M.; Beeler, T. Model-based teeth reconstruction. *ACM Trans. Graph.* **2016**, *35*, 220. [\[CrossRef\]](#)
31. Yamany, S.M.; Farag, A.A.; Tasman, D.; Farman, A.G. A 3-D reconstruction system for the human jaw using a sequence of optical images. *IEEE Trans. Med. Imaging* **2000**, *19*, 538–547. [\[CrossRef\]](#) [\[PubMed\]](#)
32. Zhan, X.; Cai, Y.; He, P. A three-dimensional point cloud registration based on entropy and particle swarm optimization. *Adv. Mech. Eng.* **2018**, *10*, 1687814018814330. [\[CrossRef\]](#)
33. Zhan, X.; Cai, Y.; Li, H.; Li, Y.; He, P. A point-cloud registration algorithm based on normal vector and particle swarm optimization. *Meas. Control* **2019**, *53*, 265–275. [\[CrossRef\]](#)
34. Ge, Y.; Wang, B.; Nie, J.; Sun, B. A point cloud registration method combining enhanced particle swarm optimization and iterative closest point method. In Proceedings of the 2016 Chinese Control and Decision Conference (CCDC), Yinchuan, China, 28–30 May 2016; IEEE: Piscataway Township, NJ, USA, 2016; pp. 2810–2815.
35. Yousry, M.; Youssef, B.A.B.; El Aziz, M.A.; Sidky, F.I. 3D Point-cloud Registration Using Particle Swarm Optimization Based on Different Descriptors. *Int. J. Sci. Eng. Res.* **2017**, *8*, 558–564.
36. John, V.; Xu, Y.; Mita, S.; Long, Q.; Liu, Z.; Tan, Y.; Takagi, H.; Shi, Y. Registration of GPS and Stereo Vision for Point Cloud Localization in Intelligent Vehicles Using Particle Swarm Optimization. In *Lecture Notes in Computer Science*; Springer International Publishing: Berlin/Heidelberg, Germany, 2017; Volume 10385, pp. 209–217.
37. Zhang, L.; Yang, B.; Wang, L.; Zhao, X.; Zhou, J.; Li, M.; Han, Y. Three-dimensional Cement Image Registration Based on Multi-layer PSO and Mutual Information. In Proceedings of the 2016 3rd International Conference on Informative and Cybernetics for Computational Social Systems (ICCSS), Jinzhou, China, 26–29 August 2016.
38. Feng, Y.; Tang, J.; Su, B.; Su, Q.; Zhou, Z. Point Cloud Registration Algorithm Based on the Grey Wolf Optimizer. *IEEE Access* **2020**, *8*, 143375–143382. [\[CrossRef\]](#)
39. Wongkhuenaew, R.; Auephanwiriyakul, S.; Chaiworawitkul, M.; Theera-Umpon, N. Three-Dimensional Tooth Model Reconstruction Using Statistical Randomization-Based Particle Swarm Optimization. *Appl. Sci.* **2021**, *11*, 2363. [\[CrossRef\]](#)
40. Mirjalili, S.; Mirjalili, S.M.; Lewis, A. Grey wolf optimizer. *Adv. Eng. Softw.* **2014**, *69*, 46–61. [\[CrossRef\]](#)
41. Singh, N.; Singh, S.B. A novel hybrid GWO-SCA approach for optimization problems. *Eng. Sci. Technol. Int. J.* **2017**, *20*, 1586–1601. [\[CrossRef\]](#)

42. Heidari, A.A.; Pahlavani, P. An efficient modified grey wolf optimizer with Lévy flight for optimization tasks. *Appl. Soft Comput.* **2017**, *60*, 115–134. [\[CrossRef\]](#)
43. Long, W.; Jiao, J.; Liang, X.; Cai, S.; Xu, M. A Random Opposition-Based Learning Grey Wolf Optimizer. *IEEE Access* **2019**, *7*, 113810–113825. [\[CrossRef\]](#)
44. Nadimi-Shahraki, M.H.; Taghian, S.; Mirjalili, S. An improved grey wolf optimizer for solving engineering problems. *Expert Syst. Appl.* **2021**, *166*, 113917. [\[CrossRef\]](#)
45. Wang, F.; Zhao, Z. A survey of iterative closest point algorithm. In Proceedings of the Chinese Automation Congress (CAC), Jinan, China, 20–22 October 2017; IEEE: Piscataway Township, NJ, USA, 2017; pp. 4395–4399. [\[CrossRef\]](#)
46. Duda, R.O.; Hart, P.E.; Stork, D.G. *Pattern Classification*, 2nd ed.; John Wiley & Sons: Hoboken, NJ, USA, 2001.
47. Chen, Y.; Medioni, G. Object modelling by registration of multiple range images. *Image Vis. Comput.* **1992**, *10*, 145–155. [\[CrossRef\]](#)
48. FitzGibbon, A.W. Robust registration of 2D and 3D point sets. *Image Vis. Comput.* **2003**, *21*, 1145–1153. [\[CrossRef\]](#)
49. Rezaei, F.; Safavi, H.R.; Abd Elaziz, M.; El-Sappagh, S.H.A.; Al-Betar, M.A.; Abuhmed, T. An Enhanced Grey Wolf Optimizer with a Velocity-Aided Global Search Mechanism. *Mathematics* **2022**, *10*, 351. [\[CrossRef\]](#)
50. Long, W.; Jiao, J.; Liang, X.; Tang, M. An exploration-enhanced grey wolf optimizer to solve high-dimensional numerical optimization. *Eng. Appl. Artif. Intell.* **2018**, *68*, 63–80. [\[CrossRef\]](#)
51. Gao, Z.-M.; Zhao, J. An Improved Grey Wolf Optimization Algorithm with Variable Weights. *Comput. Intell. Neurosci.* **2019**, *2019*, 2981282. [\[CrossRef\]](#)
52. Qiao, Y.; Hsu, H.-Y.; Pan, J.-S. Behavior-based Grey Wolf Optimizer for Wireless Sensor Network Deployment Problem. *Int. J. Ad Hoc Ubiquitous Comput.* **2022**, *39*, 70–82. [\[CrossRef\]](#)
53. Yang, X.-S. *Nature-Inspired Metaheuristic Algorithms*, 2nd ed.; Luniver Press: England, UK, 2010; ISBN 1-905986-28-9.
54. Kennedy, J.; Eberhart, R. Particle swarm optimization. In Proceedings of the International Conference on Neural Networks (ICNN), Perth, WA, Australia, 27 November–1 December 1995; pp. 1942–1948. [\[CrossRef\]](#)
55. Besl, P.; McKay, N.D. A method for registration of 3-D shapes. *IEEE Trans. Pattern Anal. Mach. Intell.* **1992**, *14*, 239–256. [\[CrossRef\]](#)
56. Lagarias, J.C.; Reeds, J.A.; Wright, M.H.; Wright, P.E. Convergence Properties of the Nelder-Mead Simplex Method in Low Dimensions. *SIAM J. Optim.* **1998**, *9*, 112–147. [\[CrossRef\]](#)
57. Arora, S.; Singh, S. Butterfly optimization algorithm: A novel approach for global optimization. *Soft Comput.* **2019**, *23*, 715–734. [\[CrossRef\]](#)
58. Heidari, A.A.; Mirjalili, S.; Faris, H.; Aljarah, I.; Mafarja, M.; Chen, H. Harris hawks optimization: Algorithm and applications. *Future Gener. Comput. Syst.* **2019**, *97*, 849–872. [\[CrossRef\]](#)
59. Li, S.; Chen, H.; Wang, M.; Asghar Heidari, A.A.; Mirjalili, S. Slime mould algorithm: A new method for stochastic optimization. *Future Gener. Comput. Syst.* **2020**, *111*, 300–323. [\[CrossRef\]](#)
60. Mirjalili, S.; Lewis, A. The Whale Optimization Algorithm. *Adv. Eng. Softw.* **2016**, *111*, 300–323. [\[CrossRef\]](#)
61. Li, P.; Wang, R.; Wang, Y.; Gao, G. Fast Method of Registration for 3D RGB Point cloud with Improved Four Initial Point Pairs Algorithm. *Sensors* **2020**, *20*, 138. [\[CrossRef\]](#)
62. Du, S.; Zheng, N.; Xiong, L.; Ying, S.; Xue, J. Scaling iterative closest point algorithm for registration of m-D point sets. *J. Vis. Commun. Image Represent.* **2010**, *21*, 442–452. [\[CrossRef\]](#)
63. Glira, P.; Pfeifer, N.; Ressel, C.; Briese, C. A correspondence framework for ALS strip adjustments based on variants of the ICP algorithm. *J. Photogramm. Remote Sens. Geoinf. Sci. (PFG)* **2015**, *4*, 275–289. [\[CrossRef\]](#)
64. Glira, P.; Pfeifer, N.; Ressel, C.; Briese, C. Rigorous Strip Adjustment of Airborne Laser scanning Data Based on the ICP Algorithm. *ISPRS Ann. Photogramm. Remote Sens. Spat. Inf. Sci.* **2015**, *2*, 73–80. [\[CrossRef\]](#)
65. Point Cloud Tools for Matlab. Available online: www.geo.tuwien.ac.at/downloads/pg/pctools/pctools.html (accessed on 12 May 2022).
66. Kalla, M.-P.; Economopoulos, T.L.; Matsopoulos, G.K. 3D dental image registration using exhaustive deformable models: A comparative study. *Dentomaxillofacial Radiol.* **2017**, *46*, 20160390. [\[CrossRef\]](#)
67. Kim, M.; Chung, M.; Shin, Y.-G.; Kim, B. Automatic registration of dental CT and 3D scanned model using deep split jaw and surface curvature. *Comput. Methods Programs Biomed.* **2023**, *233*, 107467. [\[CrossRef\]](#)
68. Kurniawan, A.; Yodokawa, K.; Kosaka, M.; Ito, K.; Sasaki, K.; Aoki, T.; Suzuki, T. Determining the effective number and surfaces of teeth for forensic dental identification through the 3D point cloud data analysis. *Egypt. J. Forensic Sci.* **2020**, *10*, 3. [\[CrossRef\]](#)
69. Chung, M.; Lee, J.; Song, W.; Song, Y.; Yang, I.-H.; Lee, J.; Shin, Y.-G. Automatic Registration Between Dental Cone-Beam CT and Scanned Surface via Deep Pose Regression Neural Networks and Clustered Similarities. *IEEE Trans. Med. Imaging* **2020**, *32*, 3900–3909. [\[CrossRef\]](#)
70. Porumb, I.C.; Leucuta, D.C.; Nigoghossian, M.; Culic, B.; Lucaciu, P.O.; Culic, C.; Badea, I.C.; Leghezeu, A.N.; Nicoara, A.G.; Simu, M.R. Caries Lesion Assessment Using 3D Virtual Models by Examiners with Different Degrees of Clinical Experience. *Medicina* **2023**, *59*, 2157. [\[CrossRef\]](#)

Disclaimer/Publisher’s Note: The statements, opinions and data contained in all publications are solely those of the individual author(s) and contributor(s) and not of MDPI and/or the editor(s). MDPI and/or the editor(s) disclaim responsibility for any injury to people or property resulting from any ideas, methods, instructions or products referred to in the content.